Journal of Cleaner Production 211 (2019) 874–883

Contents lists available at ScienceDirect

Journal of Cleaner Production

journal homepage: www.elsevier.com/locate/jclepro

Novel low temperature synthesis of sodium silicate and ordered mesoporous silica from incineration bottom ash

Qadeer Alam[*, 1], Yuri Hendrix [1], Luuk Thijs, Alberto Lazaro, Katrin Schollbach, H.J.H. Brouwers

Department of the Built Environment, Eindhoven University of Technology, P. O. Box 513, 5600, MB, Eindhoven, the Netherlands

ARTICLE INFO

Article history:
Received 13 August 2018
Received in revised form
11 November 2018
Accepted 19 November 2018
Available online 23 November 2018

Keywords:
Water-glass
Mesoporous silica
Bottom ash
Rietveld analysis
Sodium silicate
MSWI

ABSTRACT

A novel low temperature synthesis route to convert environmentally harmful silica-rich waste incineration bottom ashes into ordered mesoporous silica is reported. Bottom ash is a major by-product of municipal solid waste incineration with limited recycling options due to harmful contaminants. In this study, a low temperature alkaline dissolution process was employed to synthesize sodium silicate instead of a conventional high temperature fusion process. Moreover, the dissolution process was systematically investigated to attain fundamental insight into the hydrolysis of silica from bottom ash, which is currently lacking in the existing literature. The mineralogical composition of the ash residues before and after desilication experiments was quantified via Rietveld analysis to understand the formation of by-products, such as geopolymeric gels and zeolites. These by-products hinder the dissolution of the silica because of the following two factors: Firstly, their formation consumes part of the soluble silicate and, secondly, the precipitation of the by-products around the etching particles of bottom ash act as a passivating layer which hinders the diffusion of soluble silica away from the particle. The optimized reaction temperature and reaction time for the silica extraction was observed to be 75 °C for 48 h. A sequential extraction under these conditions can successfully attain an extraction efficiency of 70% of the silica. Subsequently, the sodium silicate derived from the bottom ash was used to synthesize mesoporous silica with a high specific surface area and purity of 870 m^2/g and 99 wt %, respectively.

1. Introduction

Mesoporous silica structures are an important material group, that can be applied as specialized catalysts (Dworakowska et al., 2017), adsorbents or used in drug delivery (Slowing et al., 2008) and molecular separation (Xu et al., 2018). These applications are made possible because mesoporous silica has a large specific surface areas (SSA) of 1000 m^2/g and pores between 2 and 50 nm. While naturally occurring zeolites also have large SSA, the well-defined and modifiable porous network of mesoporous structures with pores larger than 2 nm is crucial for the aforementioned applications. The first mesoporous silica products were made by hydrothermal treatment of aluminosilicate gels with a crystal liquid template formed by surfactants (Kresge et al., 1992). Since then the research on mesoporous silica have expanded extensively. A few years later Stucky and his team described more general and easier pathways to form these structures with a cooperative assembly method using either silicon alkoxides or silicate solutions as silica precursors (Huo et al., 1994). From these, sodium silicate is the more low cost resource, which is important due to the ever-increasing production.

In addition to mesoporous silica, sodium silicate (also known as water-glass) is used to produce zeolites (Chiang et al., 2012), detergents (de Lucas et al., 2002) and building materials (Kamseu et al., 2017). In terms of volume, sodium silicate is the most extensively used as industrial raw material after acids and bases (Van Dokkum et al., 2004). However, the current industrial production method requires an immense energy input. The major production method is fusing sodium carbonate with high quality quartz sand at temperatures between 1300 °C and 1600 °C (Lazaro et al., 2013). Therefore, the synthesis of sodium silicate and precipitated silica from silica rich industrial by-products is being intensively explored. In the literature, the recovery of silica from different ashes as coal combustion ashes (Chandrasekar et al., 2008;

* Corresponding author.
E-mail address: q.alam@tue.nl (Q. Alam).
[1] Both authors contributed equally.

https://doi.org/10.1016/j.jclepro.2018.11.173
0959-6526/

Nomenclature

BA	Bottom ash
BET	Brunauer-Emmett-Teller
BJH	Barett Joyner Halenda
CTAB	Cetyltrimethylammonium bromide
DSC	Differential scanning calorimetry
EDS	Energy dispersive X-ray spectroscopy
EE	Extraction efficiency
FTIR	Fourier transformed infrared spectroscopy
ICP-OES	Inductively coupled plasma-optical emission spectroscopy
L/S	Liquid to solid ratio
MSWI	Municipal solid waste incineration
SEM	Scanning electron microscopy
SSA	Specific surface area
TBA	Treated bottom ash
TEM	Transmission electron microscopy
XRD	X-ray diffraction
XRF	X-ray fluorescence spectrometry

Li and Qiao, 2016), biomass bottom ash (Dodson et al., 2013), rice husk ash (Tong et al., 2018) has been reported. However, the extractions in these studies were performed with conventional fusion methods utilizing high temperatures. Hence, investigating a low temperature synthesis route to extract silica from a problematic incineration ash could provide an alternative production process.

Bottom ash (BA) originating from municipal solid waste incineration (MSWI) is a silica rich residue, which is a good candidate for the synthesis of sodium silicate due to its high silica content and easy availability. In 2014, the total quantity of the BA produced in the EU was 18 million tonnes (CEWEP, 2016). BA is a complex mineralogical mixture containing a variety of contaminants (Alam et al., 2017) such as heavy metals, which make their recycling challenging. Currently, these ashes are being recycled in form of loose aggregates, adsorbents (Luo et al., 2017), ceramics (Bourtsalas et al., 2015), blended cement (Li et al., 2012) and alkali activated materials (Silva et al., 2017). However, to the best of the authors' knowledge, there is only one reported study in which MSWI bottom ash was utilized for the recovery of silica. Liu et al. (2014) has reported the extraction of silica from BA by fusing it with $LiBO_2$ at a temperature of 900 °C. The aforementioned study focuses mostly on the silica extraction efficiency instead of the reaction mechanism and limiting factors that affect the dissolution of silica. The complex mineralogy and heterogeneity of these ashes make it difficult to obtain a clear insight into the dissolution mechanism and kinetics. The fundamental understanding of the extraction process of silica and accompanying changes in the mineral composition are not well understood. Furthermore, it would be desirable from an economic and environmental point of view if the dissolution of silica from these incineration ashes can be achieved at a low temperature.

In this study, a low temperature synthesis of sodium silicate by using MSWI bottom ash as a silica source, and its subsequent use in the production of mesoporous silica is reported for the first time. For this purpose, an in-depth characterization of the BA was performed via Rietveld analysis. During the extraction process, the mineralogical changes in the BA residues were quantified to identify the dissolution mechanism of silica and the side reactions which hinder the complete dissolution. In addition, the sodium silicate solution produced from the ash was utilized for the production of high purity mesoporous silica to demonstrate that the incineration ash can be recycled by producing high quality silica products.

2. Materials and methods

2.1. Materials

The Heros Sluiskil company (the Netherlands) provided the MSWI bottom ash used in this study. This material was weathered for 2 months after water quenching and then underwent magnetic separation and advanced dry recovery to remove ferrous and non-ferrous materials, respectively. Subsequently, the BA fraction 4–12 mm was obtained via dry sieving at the company and used in this study, because of its high SiO_2 content. The BA fraction (4–12 mm) was milled in the lab in a planetary ball mill (Fritsch; Pulverisette 5) below 125 μm.

All the chemicals used in this study were of analytical grade and used as received without any further purification. Sodium hydroxide pellets, 70 vol % nitric acid, 37 vol % hydrochloric acid and Cetyltrimethylammonium bromide (CTAB) were obtained from Sigma Aldrich, the Netherlands.

2.2. Characterization methods

The chemical composition of the BA was analyzed with an X-ray fluorescence spectrometer (XRF; PANalytical Epsilon 3) by using fused beads. Prior to analysis, the loss on ignition of BA was measured at 600 °C for 7 h to obtain constant mass. Afterwards, BA was mixed with a flux ($Li_2B_4O_7$ and $LiBO_4$) in the presence of a wetting agent (LiBr) and the melt was prepared in a fluxer oven (clasisse leNeo) at 1100 °C. This melt was used to cast fused bead which was later analyzed with XRF to obtain the chemical composition of the sample.

The mineral compositions of the original BA and the residues collected after the extraction experiments were determined with X-Ray diffraction (XRD). Samples for XRD analysis were milled below 10 μm and 10 wt % of Si was added as an internal standard for the quantification of the crystalline and amorphous phases. The diffraction patterns of the samples were obtained between the ranges of 5–90° 2θ with a measurement step size of 0.02 by using a D2 diffractometer from Bruker. The diffractometer was equipped with Co-Tubes ($K_{\alpha 1}$:1.7901 Å and $K_{\alpha 2}$: 1.7929 Å), a LynxEye detector, divergence slit of 0.2° and soller slits of 2.5°. The identification of phases was carried out with a software (X'Pert HighScore Plus 2.2) from PANalytical which was equipped with a ICDD PDF-2 database. After the identification of the phases a Rietveld analysis was performed for the quantification of the crystalline phases and amorphous content with the help of the TOPAS software (version 4.2) from Bruker (Coelho, 2018). The crystal structures used for the refinement were obtained from the ICSD database (FIZ Karlsruhe). In order to ensure the accuracy of the Rietveld analysis, the content of quartz in the BA was quantified independently and used as an external reference. The α-β inversion thermal transition of quartz at 573 °C was measured with a heating and cooling rate of 10 °C min^{-1} using differential scanning calorimetry (DSC 822e; Mettle Toledo). After two consecutive heating cycles between 500 and 600 °C, the cooling peak was used for the determination of the quartz content (Fig. A1).

After the extraction experiments, liquid samples were obtained by filtration and acidified using 0.2 vol% of 15 M ultrapure HNO_3. The chemical composition of the sodium silicate solution was measured with inductively coupled plasma-optical emission spectroscopy (ICP-OES; Varian 730-ES).

2.3. Silica extraction

The BA was pretreated in the presence of 4 M nitric acid. A ratio of 1: 3 (wt: vol) between BA and nitric acid was used and the mixture was stirred for 24 h at 20 °C, respectively. After this pretreatment, the mixture was left standing for 48 h to facilitate the precipitation of dissolved silica species. Subsequently, the mixture was filtered to separate the treated bottom ash (TBA) and later TBA was used for the silica extraction experiments. This acidic pretreatment can be performed in presence of any strong mineral acid; however, in this study nitric acid was used because it prevents the co-precipitation of solid by-products, such as gypsum in the case of sulfuric acid. To investigate the mineral transformation of the ash residues after the extraction experiments, it was necessary to avoid precipitation of new phases during the acid treatment.

The dissolution of silica from the TBA was studied by varying the reaction time (24, 48 and 72 h), temperature (20, 75 and 90 °C) and liquid-to-solid ratio (L/S: 25 and 50) to ascertain the optimal conditions for silica extraction. Initial extraction experiments were performed by adding TBA to NaOH with a mass ratio of 1: 0.8 in water with L/S ratio of 50 to investigate the effects of the reaction time and temperature on the dissolution of silica. The higher L/S ratio of 50 was used to avoid oversaturation during extraction and maximize the soluble silica content. The residue after the extraction experiments was carefully filtered and analyzed via XRF to quantify the remaining silica. To calculate the extraction efficiency (EE) of an experiment, only the potentially soluble silica was taken in to account which was determined by subtracting the amount of quartz from the total silica content in the BA. Quartz is known to be inert under these conditions, so it was not considered in the total available silica content. The extraction efficiency was calculated by taking the difference between the potentially available silica (excluding quartz) and the silica content that remained after the extraction experiment.

$$EE(\%) = \left(1 - \frac{SiO_{2\ residue}}{SiO_{2\ total} - SiO_{2\ quartz}}\right) \times 100 \quad (1)$$

The effect of reaction time and temperature was then analysed by comparing their EE with each other. Once the optimal reaction time and temperature for the extraction experiments were ascertained, the L/S ratio of the system was reduced to 25 while keeping the TBA to NaOH ratio constant to obtain higher concentration of soluble silica in the extraction medium. The sodium silicate solution obtained via this protocol was then further used for the synthesis of mesoporous silica.

2.4. Synthesis of mesoporous silica

The cooperative self-assembly mechanism method was used for the preparation of mesoporous silica following the S^+I^- route. CTAB was used as the cationic surfactant and was added to the silicate solution extracted from BA using the optimal conditions (48 h 75 °C). The molar ratio of CTAB to silicate was chosen to be 0.16:1, the optimum ratio as reported by Yan et al. (2016). The starting concentration of the silicate solution was measured to be 0.2 M, which is a typical concentration for the synthesis of silica structures from sodium silicate solution. This mixture was heated to 80 °C for two hours. After these two hours, the pH of the solution was slowly lowered over the course of 3 h with a 2 M hydrochloric acid until a pH value of 9 was reached. The formed suspension was transferred to a closed container and left to age for 72 h at room temperature. The aged precipitate was then filtered and washed with de-ionized water and finally calcined at 650 °C to remove the remaining surfactants.

The characterization of mesoporous silica was carried out in terms of specific surface area (SSA), purity and structure. Nitrogen physisorption was performed with a Tristar II equipment at 77 K to determine SSA using the Brunauer-Emmett-Teller (BET) theory and pore size distribution using the Battet, Joyner and Halenda (BJH) theory. To determine long-range structure of the mesoporous silica a low angle X-ray diffraction pattern (1–8° 2θ) was measured with a D2-XRD from Bruker equipped with beam knife (0.5 mm), 0.1° divergence slit and 2.5° soller slits. Transmission Electron Microscopy (TEM) was performed using a Tecnai 20 microscope equipped with a LaB6 filament, operated at 200 kV the sample was put on a 200 mesh copper grid with a carbon support layer.

3. Results and discussions

3.1. Characterization of BA

In Table 1 the bulk chemical composition of BA is provided showing that SiO_2 is the major constituent of the ash, comprising up to 59 wt %. In addition to other major oxides, BA contains a range of potentially leachable elements: Ti, Zn, Cu, Ba, Pb, Cr and Mn. The crystalline phases in BA can be categorized in three groups: 1) silicates: albite, diopside, melilite and quartz, 2) carbonates: calcite and dolomite and 3) iron oxides: magnetite and hematite (Fig. 1a). Overall, only 19 wt % of the ash consist of crystalline phases and the rest (81 wt %) is amorphous. Earlier studies reported that amorphous phases in BA includes bottle glass (del Valle-Zermeño et al., 2017) and melilitic slag (Schollbach et al., 2016). The presence of a high amorphous content and the silicate minerals makes this fraction of BA ideal for the extraction of silica. Under the alkaline conditions, the dissolution of the amorphous content and soluble silicate phase such as melilite is expected. The contribution of other well crystalline silicate phases (quartz, albite and diopside) towards the soluble silica is considered negligible due to their much lower solubility.

3.2. Pretreatment of BA

Due to the presence of contaminants, an acid pretreatment of BA was performed to extract heavy metals and to increase SSA of the ash particles to assist the dissolution of silica afterwards. After the pretreatment, decomposition of carbonate minerals such as calcite and dolomite was confirmed as shown in Fig. 1b. As reported in an earlier study about BA, carbonates act as a reservoir of divalent metallic ions, especially Zn, and Cu (Piantone et al., 2004). Therefore, a reduction in the content of these metals in the BA was achieved (Table A1). Additionally, from the silicates group, melilite was completely dissolved along with a partial dissolution of albite and diopside. Subsequently, melilite dissolved during the pretreatment was recovered by allowing the mixture to stand unstirred. The silicates dissolved in this step were reduced and transformed into silica with a gel like structure due to the polymerization in an acidic environment (Terry, 1983). The silica in gel form was separated along with the ash residues via filtration. As a result, minimal loss of silica (2 wt %) during the acid pretreatment was observed and the treated bottom ash (TBA) contained 57 wt %

Table 1
Chemical composition of original BA and acid treated BA (TBA) in wt. %. LOI: loss on ignition, LOD: loss on dissolution after acid pretreatment.

	SiO_2	CaO	Al_2O_3	Fe_2O_3	Na_2O	MgO	K_2O	Rest	LOI	LOD
BA	58.8	15.8	8.8	4.6	3.1	1.9	1.0	3.5	2.7	–
TBA	56.9	10.3	6.7	3.6	2.4	1.4	0.8	1.5	2.9	13.4

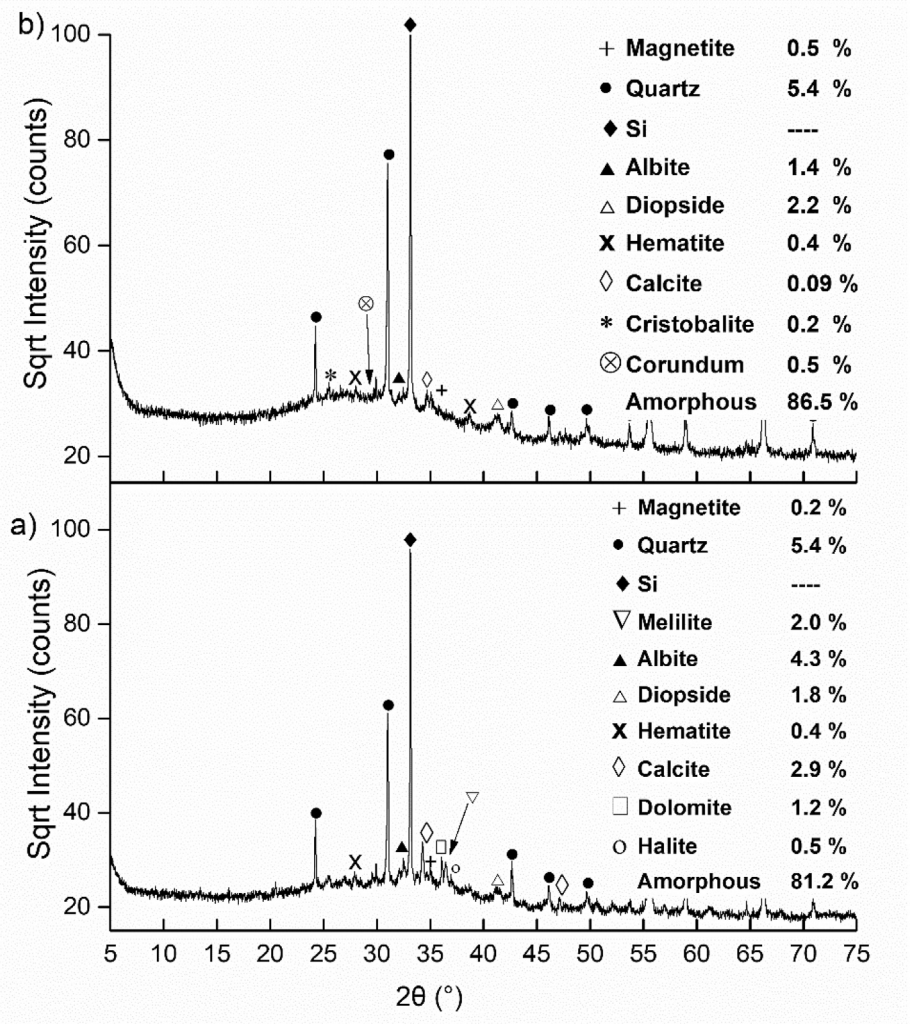

Fig. 1. XRD diffractogram and mineral quantification of a) original BA and b) BA after the acid pre-treatment (TBA).

of SiO_2, as shown in Table 1. It is worthy of note that the amorphous content (determined with quantitative XRD: Fig. 1b) of the TBA increased by 5 wt %. This increase confirms the dissolution of crystalline melilite during the acid pretreatment and its precipitation as an amorphous phase. Additionally, the dissolution of other crystalline phases (calcite & dolomite) can also contribute to the increase in the amorphous content. Furthermore, the SSA of the TBA increased more than 12 times (from 2.2 to 27.2 m^2/g). This increase in amorphous silica and SSA is expected to enhance the dissolution of silica from the ash residues obtained after acid treatment.

3.3. Silica extraction

The extraction experiments with the TBA were performed to understand the dissolution behaviour of silica and the formation of secondary silicate species. The effect of reaction time and temperature was investigated to find the optimum conditions to achieve maximum recovery of silica. The EE of these experiments under the varying times and temperatures are provided in Fig. 2. Approximately, 20% of the available silica was dissolved at 20 °C during the first 24 h. The dissolution of silica at 20 °C increased twofold when the reaction time was doubled from 24 to 48 h. Moreover, when the reaction was carried out for 72 h under the same conditions, it

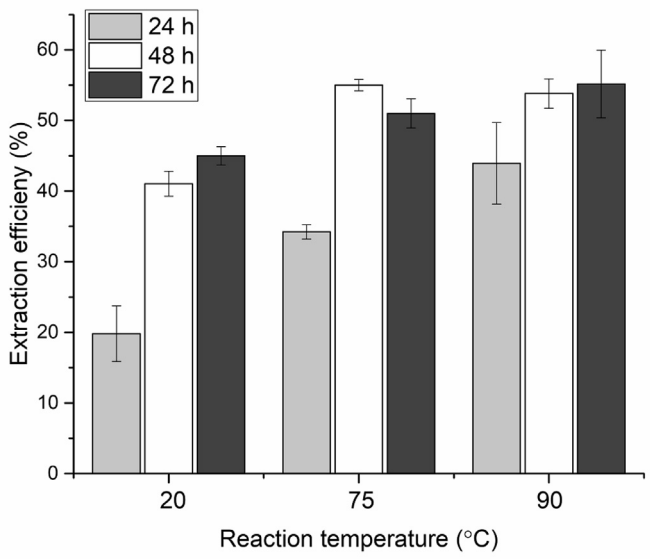

Fig. 2. Effect of reaction time and temperature on the extraction efficiency (EE) of SiO_2 from MSWI bottom ash, extraction experiments were performed with the L/S of 50.

resulted in only a minor increase for the EE. The initial source of dissolved silica can be attributed to the silicate mineral melilite; a sorosilicate with isolated double tetrahedrons. A small quantity (2 wt %) of crystalline melilite was observed in the original BA (Fig. 1a). Furthermore, previous studies suggests that in addition to crystalline melilite, the BA particles are also covered in x-ray amorphous melilitic incineration slag (Schollbach et al., 2016). This slag acts as an initial source of silica during the acid pretreatment because of its amorphous nature and high solubility in acidic media. The reduction of these silicates to silica was noted during the acid treatment and this silica was precipitated and conserved for the subsequent alkaline dissolution. The increase of silicate in the solution at reaction times higher than 24 h, indicates towards the dissolution of glass from BA. The glass in BA is mostly waste bottle glass (also called soda lime glass) and dissolves under alkaline condition to produce soluble monomeric silica species e.g., (Torres-Carrasco and Puertas, 2015). However, even employing the longest reaction times (72 h) at 20 °C could only achieve an EE of 45%.

At pH > 13 glass dissolves via etching in which the silica framework is broken down by a couple catalyst reactions of the hydroxyl anions releasing soluble silica in the solution. The first steps of the dissolution happen according to Eqs. (2) and (3).

$$\equiv Si{-}O{-}Si\equiv + OH^- \rightleftarrows \equiv Si{-}OH + \equiv Si{-}O^- \quad (2)$$

$$\equiv Si{-}O^- + H_2O \rightleftarrows \equiv Si{-}OH + OH^- \quad (3)$$

Equation (3) is an equilibrium reaction in which the $\equiv Si{-}O^-$ group is protonated. For this reaction to proceed, the silica surface needs to become negatively charged so that the reaction is thermodynamically favorable. Once the silanol group is present at the silica surface, the glass framework become open to attack by the hydroxyl group to produce soluble silica species.

The use of non-ambient temperature has been reported to enhance the dissolution of glass for synthesis of sodium silicate solution under alkaline conditions (Torres-carrasco et al., 2014). Therefore, slightly higher reaction temperatures of 75 and 90 °C were selected for the desilication of the ash. It can be seen in Fig. 2 that the increase in the reaction temperature increases the EE. More than 55% of the silica was in solution when the extraction was performed at 75 °C for 48 h. Furthermore, no significant difference in the EE was noticed upon further increase of the reaction temperature to 90 °C. Consequently, the extraction time of 48 h and a temperature of 75 °C were found to be the optimum conditions for ash desilication. However, even under these conditions only half of the potentially soluble silica was extracted which indicates that limiting factors are hindering the dissolution process.

In an alkaline media glass dissolution depends on the transfer of soluble silica species away from the etching glass particles (Strachan, 2001). Under these conditions, glass keeps on dissolving until the precipitation of secondary silicate species creates a layer on the glass surface. Due to the formation of this layer, the mass transfer will be hindered, thus slowing down the overall dissolution process (Fournier et al., 2014; Lazaro et al., 2015). In our investigation, a similar phenomenon was observed which limits the dissolution of silica. Fig. 3 shows a glass particle covered by the newly formed silicate species effectively covering the surface of glass.

The mineralogical transformations in the ash after the desilication were examined and quantified via the Rietveld method using powder XRD. The ash residues from the most successful extraction experiment (duration 48 h) were chosen and the effect of reaction temperature (20, 75 and 90 °C) on the mineral composition was studied (Fig. 4). The amorphous content of the residue obtained from the desilication experiment at 20 °C was 70.6 wt % (Fig. 4a).

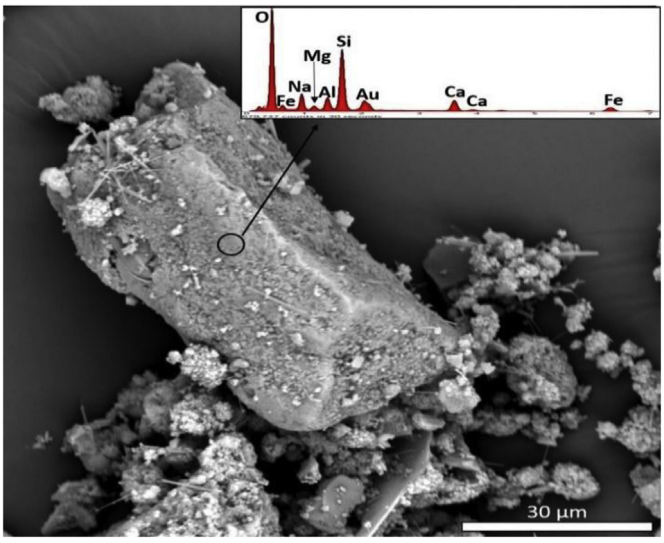

Fig. 3. SEM image (kV: 15) showing the morphology of a glass particle identified in the ash after the extraction experiments. It shows formation of the reaction products on the surface. Inset presents EDS spectrum of the encircled area on the surface of glass.

The dissolution of amorphous content increased with a higher reaction temperature of 75 °C, but still a significant amorphous content (63 wt %) remained in the residues (Fig. 4b). This indicates that even under these optimal conditions (where maximum EE was attained) complete dissolution of amorphous content was not achieved. Likewise, when extraction experiments were performed at 90 °C, the amorphous content of the ash reduced significantly and only 29.7 wt % of the amorphous content remained in the residues. However, it is worthy of note that the increase in the dissolution of amorphous content at 90 °C did not result in an increase in the EE. It was also observed that the effect of the reaction temperature and the dissolution of amorphous phases are directly proportional to each other. Under these conditions, an EE of 54% was noted, which is similar to EE achieved at the low temperature of 75 °C (Fig. 2).

The diffraction pattern of the residues obtained after the extraction experiment at 90 °C (Fig. 4c) reveals the formation of zeolites as a by-product. In our experiments, Zeolite P and Zeolite ZK14 were identified in the residue as a major (12.2 wt %) and minor (0.2 wt %) undesired by-products, respectively. These zeolites are sodium aluminosilicates and their formation is reported to occur under hydrothermal conditions at 90 °C (Du et al., 2011). The presence of these zeolites in the residues indicates that the extraction solution had sufficient amounts of reactive Al^{3+} and silicate ions for the zeolite formation (Strachan and Croak, 2000). The solubility of glass is reported to increase dramatically with the precipitation of zeolites, which is in agreement with our findings (Fournier et al., 2017). The zeolite formation readily consumes the soluble silicate species and tilts the equilibrium in favour of further glass dissolution. Thus, more glass is dissolved to compensate for the soluble silica consumed by the precipitation of secondary silicates species. Therefore, this undesired formation of zeolite decreases the amount of silica in the solution. Additionally, the formation of carbonation products; calcite and vaterite was also observed in all of the residues after the desilication experiments. The presence of $Ca(OH)_2$ is expected due to the dissolution of the amorphous content, which takes up CO_2 from the atmosphere leading to the formation of carbonate species.

Sequential extraction of silica was performed to attain a higher extraction efficiency of silica from TBA. The extraction was

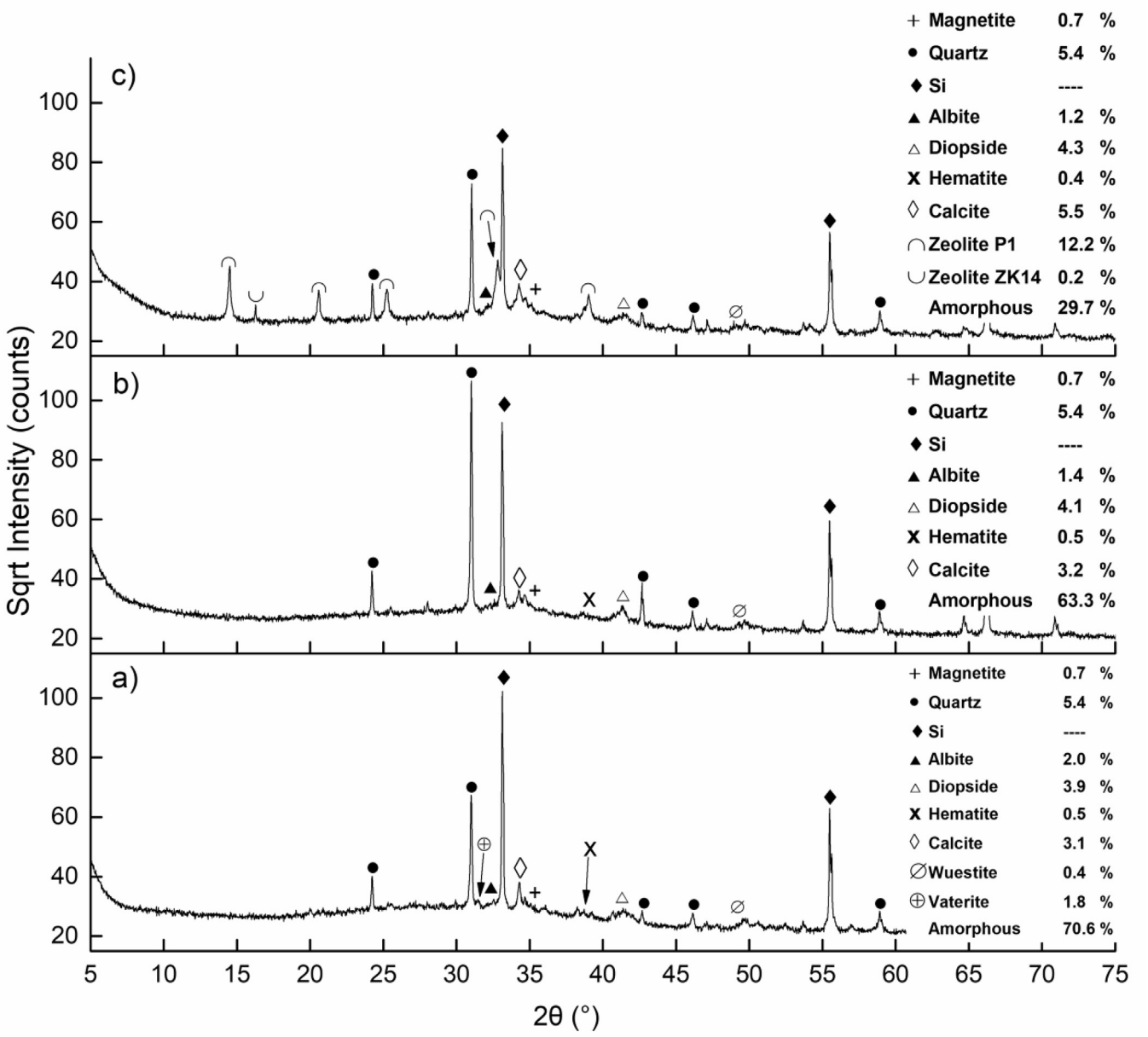

Fig. 4. XRD diffractogram and quantification of mineral phases present in the ash residues recovered after the extraction experiments with L/S of 50 for the duration of 48 h at different reaction temperatures a) 20 °C, b) 75 °C and c) 90 °C.

performed under optimal conditions (at 75 °C and 48 h) with L/S ratio of 25, which was half of the L/S used in the initial dissolution experiments. During the extraction, the equilibrium exists between the silica species in solution and secondary precipitated silicate species. According to Le Chatelier's principle, the removal of dissolved silica from the extraction system will shift the equilibrium in favour of soluble silicates, thus resulting in a higher cumulative EE. Therefore, the use of multiple steps is expected to increase the dissolution of glass from BA, resulting in higher cumulative EE. The mineralogical transformation in the ash residues after the successive extraction experiment was investigated and is displayed in Fig. 5. The analysis of Fig. 5a and b provides the mineral composition of the residue obtained after the first two steps of extractions. After two successive extraction steps, only 37 wt % of the amorphous content was left in the residues as shown in Fig. 5b. With multiple steps, an EE of more than 80% was achieved as illustrated in Fig. 5c. If the initial amorphous content of the TBA is compared with the amorphous content left after the second extraction step, then 57% of the original amorphous content was dissolved. As discussed earlier, most of the soluble silicates originate from the amorphous phases, and therefore these numbers can be compared with the cumulative EE efficiency of 68% (shown in Fig. 5c) achieved after the second extraction step. The difference between the overall decrease in the amorphous content and the achieved EE is explained by the formation of zeolite P and carbonation products after the extractions. The formation of these products increases the crystalline components in the ash residues, affecting the ratio of crystalline to amorphous content.

Furthermore, the reduction of the L/S ratio to 25 led to the formation of zeolite P at a lower temperature of 75 °C. This is contrary to the experiments performed at a higher L/S of 50 where no zeolite precipitation was observed at the same temperature. This indicates

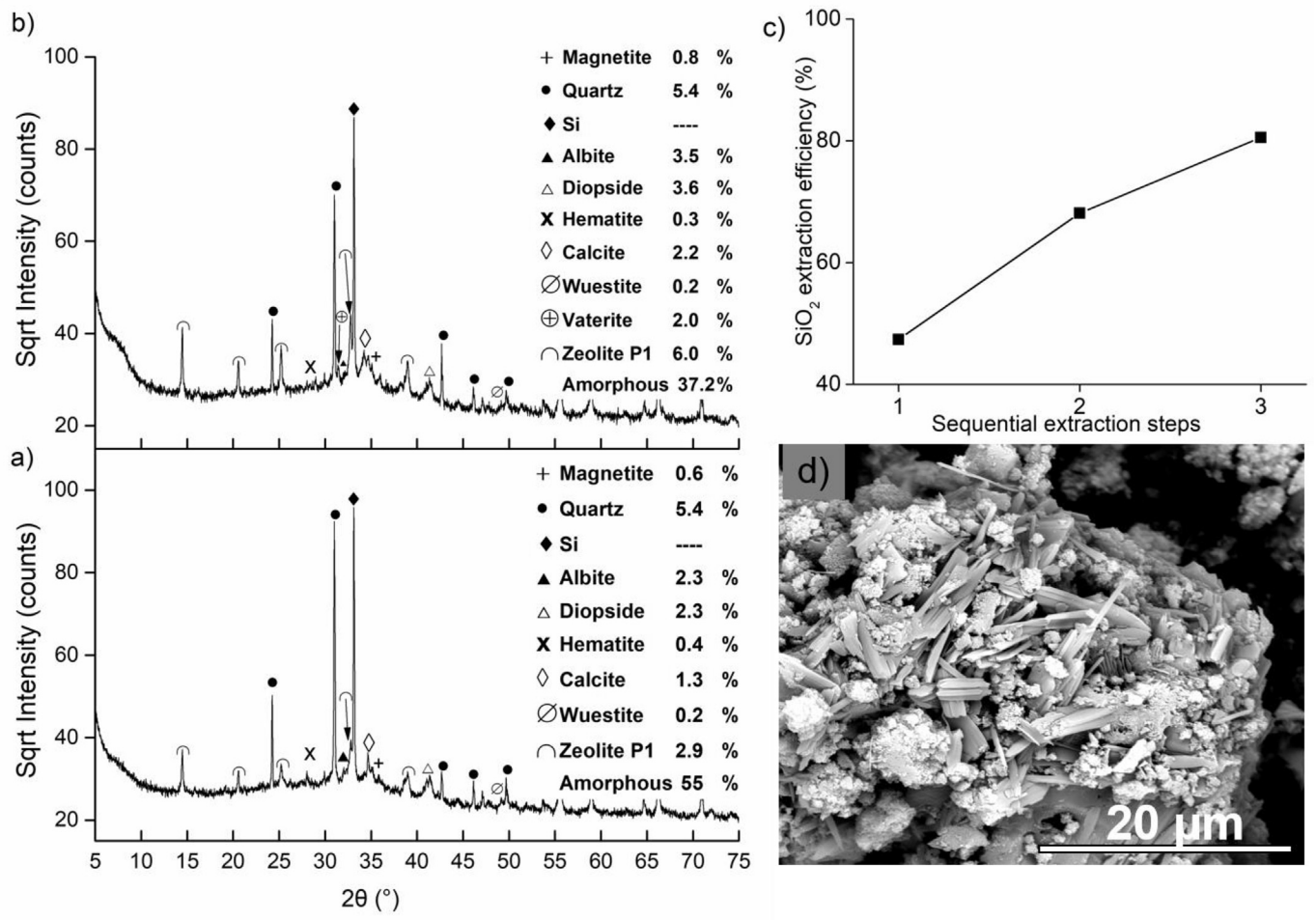

Fig. 5. a) Diffraction pattern and mineral quantification of the ash residues after first step **b)** after second step, c) cumulative extraction efficiency of SiO_2 from bottom ash and **d)** SEM image (kV: 20, magnification: 6129×) showing morphology of the zeolites and geopolymeric gels formed during extraction. The extraction experiments were performed for the duration of 48 h at 75 °C with L/S of 25.

that by reducing the total volume the reaction mixture becomes saturated with ions playing a vital role in the precipitation of the zeolite, thus enhancing the dissolution of glass and releasing more silica in the solution. The precipitated zeolite (Fig. 5d) shows needle like structures. According to literature, Zeolite P has the chemical formula of $Na_{3.5}(Al_{3.6}Si_{12.4}O_{32})(H_2O)_{10.6}$ with Si/Al ratio of 3.4 (Håkansson et al., 1990). The Si/Al ratio of the needle shaped crystals observed in the current study was 3.5 (measured with EDS), which is in accordance with previously reported values. Furthermore, EDS also showed a much higher content of Na in the zeolite which can be explained by the presence of NaOH in the extraction medium. Furthermore, Fig. 5d shows reaction products in addition to the zeolites. The dissolution of Si and Al species from MSWI bottom ash under these alkaline conditions can also lead to the formation of alkaline aluminosilicates gel such as C-A-S–H and N-A-S–H (Gao et al., 2017; Wongsa et al., 2017). The high content of Na in the solution as compared to Ca along with the precipitation of Na-rich zeolites indicates that the N-A-S–H gel is prevalent under the extraction conditions. N-A-S–H gel is considered as a precursor of zeolites (Alonso and Palomo, 2001) and its formation is reported upon addition of glass to the alkali activated geopolymeric systems (Torres-Carrasco and Puertas, 2015). However, it is not possible to differentiate between N-A-S–H and other amorphous phases via XRD.

The chemical composition of the sodium silicate obtained after the first extraction step is presented in (Table A2). The concentration of SiO_2 and Na_2O in the extraction solution was 0.2 and 0.33 molar, respectively, resulting in a SiO_2/Na_2O molar ratio of 0.6. Furthermore, traces of other heavy metals (Fe: 0.02, Cu: 0.02, Pb: 0.03, Sb: 0.07, Zn: 0.02 mg/L) were also noted.

3.4. Mesoporous silica

The formation of the mesoporous silica followed the S^+I^- route (Huo et al., 1994), which posits that the formation of mesoporous structure happens through the polymerization of silicate species that are absorbed by the cationic surfactant head groups through coulomb forces. The elemental composition (Table A3) and FTIR spectra (Fig. A2) of the final product show that most of the precipitate consisted of SiO_2 species. Most likely, the contaminants present in the extracted silicate solution did not precipitate and were washed away during filtration making the mesoporous silica to have a high purity of 98.5%. The synthesis yield of the mesoporous silica from BA-derived sodium silicate was 47%, which means that 26% of the available silica from BA was converted into the final product. Using the BET theory, it could be calculated that the specific surface area of the mesoporous structure was 869.6 m^2/g (Thommes et al., 2015). The pore size distribution of this material in Fig. 6b shows that the porous network mostly contained pore sizes between 2 and 4 nm along with some larger pores. The

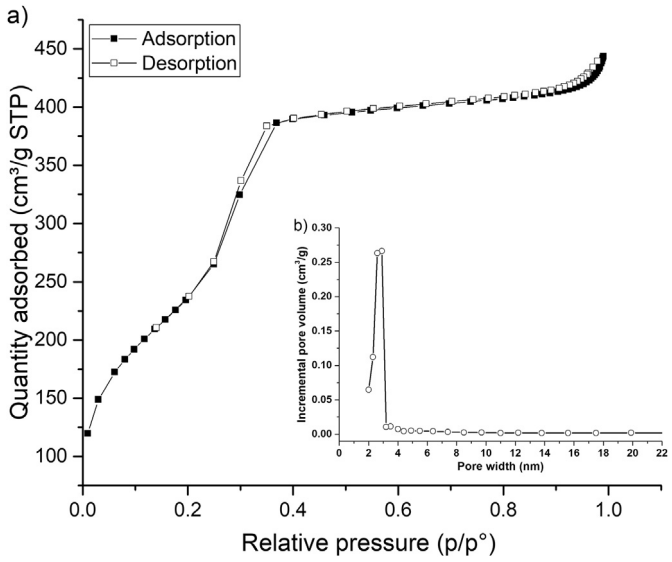

Fig. 6. a) Nitrogen physisorption isotherm and b) pore size distribution of the mesoporous silica synthesized from MSWI bottom ash.

isotherm from the nitrogen physisorption on the produced mesoporous silica is shown in Fig. 6a. The hysteresis is too small to be definable since most pores were too small (<4 nm). Therefore, the isotherm is a type IVb isotherm, which is associated with mesoporous structures with small pore sizes. The shape of the isotherm is formed by monolayer formation of adsorbed nitrogen molecules on the external surface followed by capillary condensation of the nitrogen inside the porous structure. In addition, unlike normal type IV isotherms, there is another adsorption range at the higher pressure meaning a multilayer is being formed on a large rough external surface. The small-angle X-ray diffractogram shown in Fig. 7a confirms the presence of an ordered mesostructure. Using Bragg's law, the average interplanar spacing was calculated to be 3.9 nm. This spacing includes both the pore radius and wall thickness and is common for mesoporous silica structures.

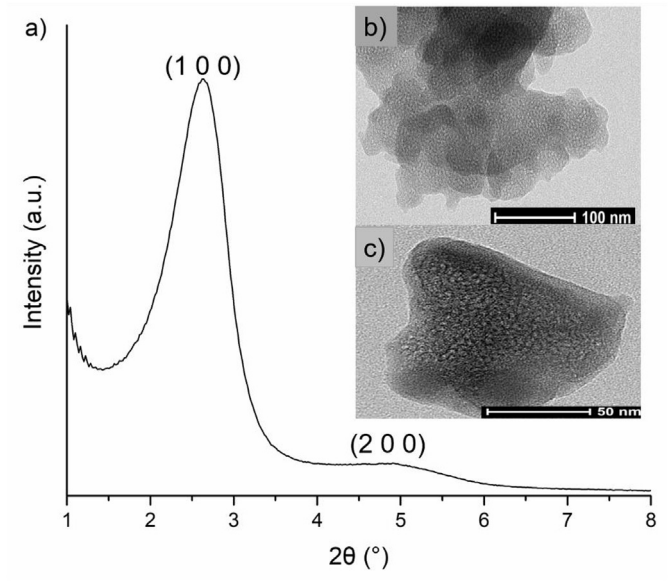

Fig. 7. a) XRD diffractogram of the mesoporous silica synthesized from MSWI bottom ash b) and c) TEM images showing internal structure.

The TEM pictures in Fig. 7b and c shows the overall structure of the produced mesoporous silica. The product contained both free colloidal particles of around 100 nm and larger micron sized agglomerates. The TEM pictures confirm that the structure has a rough large external structure. The internal porous structure is slightly more disordered than the standard porous structure of mesoporous silica. Instead of tubes in a clear hexagonal structure, the pores are more spherical with random orientations. As reported in literature, this kind of mesoporous structure can be caused by iron cations in the solution during the formation (Szegedi et al., 2004), which were present in the silicate solution (Table A2). The silicate anion attracts the cations which can either disrupted the $S^{+}I^{-}$ interaction or be incorporated into the structure during the condensation. Due to different properties like bond distance to the oxygen, defects in the structure are then produced making long ranged structure less likely. However, even with these defects, the product contains still a mesoporous structure with a large open specific surface area and high purity.

4. Conclusions and implications

A novel low temperature synthesis route for sodium silicate and mesoporous silica from environmentally harmful MSWI bottom ash is reported:

- The crystalline phases in the BA account for 19 wt % and can be grouped into: 1) Silicates (quartz, melilite, albite and diposide), 2) Carbonates (calcite and dolomite), 3) Iron oxides (magnetite and hematite) and 4) Salt (halite). The rest (81 wt %) consist of amorphous phases.
- Initial acid pretreatment was devised to reduce these undesired constituents (heavy metals and carbonates), to increase the amorphous silica by dissolving crystalline silicates (melilite) and to enhance the SSA of BA by 12 times. Hence, making the material ideal for the extraction of silica.
- In an alkaline medium, the effect of the reaction time and temperature was studied, and it was observed that a low temperature and time (20 °C and 24 h) lead to the incomplete dissolution of silica. The optimal parameters for the extraction of silica were 75 °C and 48 h. A further increase in temperature and time do not lead to a higher extraction efficiency.
- The mineralogical changes in the BA residue were quantified and the incomplete dissolution of the silica from BA is attributed to, 1) precipitation of secondary silicates species (geopolymeric gels and zeolites) during extraction and 2) the role of these products in passivating the silica rich particles and hindering the mass transfer of silica into the solution.
- By using sequential extraction under the optimal conditions, more than 70 wt % of the silica was recovered from the BA residues in the form of sodium silicate solution.
- A high quality mesoporous silica was produced from BA-derived sodium silicate solution. The synthesized mesoporous structure had a high specific surface area of 870 m^2/g and a purity of 98.5 wt %.

4.1. Implications

This study demonstrates the application potential of MSWI bottom ash as a precursor in synthesizing high-end silica products. Currently, BA is often recycled as an aggregate in concrete, a low-end application that still requires pretreatment due to contaminants. For BA producers, especially in countries like the Netherlands that have strict environmental regulations (Soil Quality Decree, 2013) and the ambition to recycle 100% of BA by

2020 (Greendeal-GD076, 2012), this novel application is of particular interest. The extraction process removes many of the contaminants present in BA and produces an inert residue as side-product, which can be used as a filler in building materials. However, to apply the finding of this study on the industrial scale, further research in upscaling the process and increasing its efficiency is needed. This study shows that transforming the environmentally harmful MSWI bottom ash into the high quality precipitated silica is a viable route for its recycling.

Declarations of interest

None.

Acknowledgements

The authors would like to acknowledge the financial support provided by NWO, the Netherlands, under the project number 10019729: “Environmental concrete based on the treated MSWI bottom ashes” and project number 10016335: “Nanoparticles for concrete”. Special thanks to V. Capari for designing graphical abstract of this paper.

Appendix A: Supplementary data

Supplementary data to this article can be found online at https://doi.org/10.1016/j.jclepro.2018.11.173.

References

Alam, Q., Florea, M.V.A., Schollbach, K., Brouwers, H.J.H., 2017. A two-stage treatment for Municipal Solid Waste Incineration (MSWI) bottom ash to remove agglomerated fine particles and leachable contaminants. Waste Manag. 67, 181–192. https://doi.org/10.1016/J.WASMAN.2017.05.029.

Alonso, S., Palomo, A., 2001. Calorimetric study of alkaline activation of calcium hydroxide–metakaolin solid mixtures. Cement Concr. Res. 31, 25–30. https://doi.org/10.1016/S0008-8846(00)00435-X.

Bourtsalas, A., Vandeperre, L.J., Grimes, S.M., Themelis, N., Cheeseman, C.R., 2015. Production of pyroxene ceramics from the fine fraction of incinerator bottom ash. Waste Manag. 45, 217–225. https://doi.org/10.1016/j.wasman.2015.02.016.

CEWEP, 2016. Bottom ash fact sheet [WWW Document]. http://www.cewep.eu/2017/09/08/bottom-ash-factsheet/. (Accessed 20 October 2018).

Chandrasekar, G., You, K.-S., Ahn, J.-W., Ahn, W.-S., 2008. Synthesis of hexagonal and cubic mesoporous silica using power plant bottom ash. Microporous Mesoporous Mater. 111, 455–462. https://doi.org/10.1016/j.micromeso.2007.08.019.

Chiang, Y.W., Ghyselbrecht, K., Santos, R.M., Meesschaert, B., Martens, J.A., 2012. Synthesis of zeolitic-type adsorbent material from municipal solid waste incinerator bottom ash and its application in heavy metal adsorption. Catal. Today 190, 23–30. https://doi.org/10.1016/j.cattod.2011.11.002.

Coelho, A.A., 2018. *TOPAS* and *TOPAS-Academic*: an optimization program integrating computer algebra and crystallographic objects written in C++. J. Appl. Crystallogr. 51, 210–218. https://doi.org/10.1107/S1600576718000183.

de Lucas, A., Rodrıguez, L., Lobato, J., Sánchez, P., 2002. Synthesis of crystalline δ-Na2Si2O5 from sodium silicate solution for use as a builder in detergents. Chem. Eng. Sci. 57, 479–486. https://doi.org/10.1016/S0009-2509(01)00372-4.

del Valle-Zermeño, R., Gómez-Manrique, J., Giro-Paloma, J., Formosa, J., Chimenos, J.M., 2017. Material characterization of the MSWI bottom ash as a function of particle size. Effects of glass recycling over time. Sci. Total Environ. 581–582, 897–905. https://doi.org/10.1016/J.SCITOTENV.2017.01.047.

Dodson, J.R., Cooper, E.C., Hunt, A.J., Matharu, A., Cole, J., Minihan, A., Clark, J.H., Macquarrie, D.J., 2013. Alkali silicates and structured mesoporous silicas from biomass power station wastes: the emergence of bio-MCMs. Green Chem. 15, 1203. https://doi.org/10.1039/c3gc40324f.

Du, Y., Shi, S., Dai, H., 2011. Water-bathing synthesis of high-surface-area zeolite P from diatomite. Particuology 9, 174–178. https://doi.org/10.1016/J.PARTIC.2010.06.006.

Dworakowska, S., Tiozzo, C., Niemczyk-Wrzeszcz, M., Michorczyk, P., Ravasio, N., Psaro, R., Bogdał, D., Guidotti, M., 2017. Mesoporous molecular sieves containing niobium(V) as catalysts for the epoxidation of fatty acid methyl esters and rapeseed oil. J. Clean. Prod. 166, 901–909. https://doi.org/10.1016/J.JCLEPRO.2017.08.098.

Fournier, M., Gin, S., Frugier, P., 2014. Resumption of nuclear glass alteration: state of the art. J. Nucl. Mater. 448, 348–363. https://doi.org/10.1016/J.JNUCMAT.2014.02.022.

Fournier, M., Gin, S., Frugier, P., Mercado-Depierre, S., 2017. Contribution of zeolite-seeded experiments to the understanding of resumption of glass alteration. npj Mater. Degrad. 1, 17. https://doi.org/10.1038/s41529-017-0018-x.

Gao, X., Yuan, B., Yu, Q.L., Brouwers, H.J.H., 2017. Characterization and application of municipal solid waste incineration (MSWI) bottom ash and waste granite powder in alkali activated slag. J. Clean. Prod. 164, 410–419. https://doi.org/10.1016/J.JCLEPRO.2017.06.218.

Greendeal-GD076, 2012. Greendeals GD076: sustainable useful application of WtE bottom ash [WWW Document]. Dutch Minist. Infrastruct. Environ. http://www.greendeals.nl/gd076-verduurzaming-nuttige-toepassing-aec-bodemassen/. (Accessed 8 September 2016).

Håkansson, U., Fälth, L., Hansen, S., 1990. Structure of a high-silica variety of zeolite Na-P. Acta Crystallogr. Sect. C Cryst. Struct. Commun. 46, 1363–1364. https://doi.org/10.1107/S0108270189013260.

Huo, Q., Margolese, D.I., Ciesla, U., Feng, P., Gier, T.E., Sieger, P., Leon, R., Petroff, P.M., Schüth, F., Stucky, G.D., 1994. Generalized synthesis of periodic surfactant/inorganic composite materials. Nature 368, 317–321. https://doi.org/10.1038/368317a0.

Kamseu, E., Beleuk à Moungam, L.M., Cannio, M., Billong, N., Chaysuwan, D., Melo, U.C., Leonelli, C., 2017. Substitution of sodium silicate with rice husk ash-NaOH solution in metakaolin based geopolymer cement concerning reduction in global warming. J. Clean. Prod. 142, 3050–3060. https://doi.org/10.1016/J.JCLEPRO.2016.10.164.

Kresge, C.T., Leonowicz, M.E., Roth, W.J., Vartuli, J.C., Beck, J.S., 1992. Ordered mesoporous molecular sieves synthesized by a liquid-crystal template mechanism. Nature 359, 710–712. https://doi.org/10.1038/359710a0.

Lazaro, A., Benac-Vegas, L., Brouwers, H.J.H., Geus, J.W., Bastida, J., 2015. The kinetics of the olivine dissolution under the extreme conditions of nano-silica production. Appl. Geochem. 52, 1–15. https://doi.org/10.1016/J.APGEOCHEM.2014.10.015.

Lazaro, A., Quercia, G., Brouwers, H.J.H., Geus, J.W., 2013. Synthesis of a green nano-silica material using beneficiated waste dunites and its application in concrete. World J. Nano Sci. Eng. 3, 41–51. https://doi.org/10.4236/wjnse.2013.33006.

Li, C., Qiao, X., 2016. A new approach to prepare mesoporous silica using coal fly ash. Chem. Eng. J. 302, 388–394. https://doi.org/10.1016/J.CEJ.2016.05.029.

Li, X.-G., Lv, Y., Ma, B.-G., Chen, Q.-B., Yin, X.-B., Jian, S.-W., 2012. Utilization of municipal solid waste incineration bottom ash in blended cement. J. Clean. Prod. 32, 96–100. https://doi.org/10.1016/J.JCLEPRO.2012.03.038.

Liu, Z.-S., Li, W.-K., Huang, C.-Y., 2014. Synthesis of mesoporous silica materials from municipal solid waste incinerator bottom ash. Waste Manag. 34, 893–900. https://doi.org/10.1016/j.wasman.2014.02.016.

Luo, H., Wu, Y., Zhao, A., Kumar, A., Liu, Y., Cao, B., Yang, E.-H., 2017. Hydrothermally synthesized porous materials from municipal solid waste incineration bottom ash and their interfacial interactions with chloroaromatic compounds. J. Clean. Prod. 162, 411–419. https://doi.org/10.1016/j.jclepro.2017.06.082.

Piantone, P., Bodénan, F., Chatelet-Snidaro, L., 2004. Mineralogical study of secondary mineral phases from weathered MSWI bottom ash: implications for the modelling and trapping of heavy metals. Appl. Geochem. 19, 1891–1904. https://doi.org/10.1016/j.apgeochem.2004.05.006.

Schollbach, K., Alam, Q., Caprai, V., Florea, M.V.A., Van der Laan, S.R., Van Hoek, C.J.G., Brouwers, H.J.H., 2016. Combined chracterization of the MSWI bottom ash. In: Proceedings Of The Thirty-Eighth International Conference On Cement Microscopy. Lyon, France, pp. 74–84.

Silva, R.V., de Brito, J., Lynn, C.J., Dhir, R.K., 2017. Use of municipal solid waste incineration bottom ashes in alkali-activated materials, ceramics and granular applications: a review. Waste Manag. 68, 207–220. https://doi.org/10.1016/j.wasman.2017.06.043.

Slowing, I.I., Vivero-Escoto, J.L., Wu, C.-W., Lin, V.S.-Y., 2008. Mesoporous silica nanoparticles as controlled release drug delivery and gene transfection carriers. Adv. Drug Deliv. Rev. 60, 1278–1288. https://doi.org/10.1016/J.ADDR.2008.03.012.

Soil Quality Decree, 2013. Regeling Bodemkwaliteit, VROM, Den Haag: ruimte en Milieu. Ministerie van Volkshuisvesting. In: Ruimtelijke Ordeling en Milieubeheer.

Strachan, D.M., 2001. Glass dissolution: testing and modeling for long-term behavior. J. Nucl. Mater. 298, 69–77. https://doi.org/10.1016/S0022-3115(01)00572-4.

Strachan, D.M., Croak, T.L., 2000. Compositional effects on long-term dissolution of borosilicate glass. J. Non-Cryst. Solids 272, 22–33. https://doi.org/10.1016/S0022-3093(00)00154-X.

Szegedi, Á., Kónya, Z., Méhn, D., Solymár, E., Pál-Borbély, G., Horváth, Z.E., Biró, L.P., Kiricsi, I., 2004. Spherical mesoporous MCM-41 materials containing transition metals: synthesis and characterization. Appl. Catal. Gen. 272, 257–266. https://doi.org/10.1016/J.APCATA.2004.05.057.

Terry, B., 1983. The acid decomposition of silicate minerals part I. Reactivities and modes of dissolution of silicates. Hydrometallurgy 10, 135–150. https://doi.org/10.1016/0304-386X(83)90002-6.

Thommes, M., Kaneko, K., Neimark, A.V., Olivier, J.P., Rodriguez-Reinoso, F., Rouquerol, J., Sing, K.S.W., 2015. Physisorption of gases, with special reference to the evaluation of surface area and pore size distribution (IUPAC Technical Report). Pure Appl. Chem. 87, 1051–1069. https://doi.org/10.1515/pac-2014-1117.

Tong, K.T., Vinai, R., Soutsos, M.N., 2018. Use of Vietnamese rice husk ash for the production of sodium silicate as the activator for alkali-activated binders. J. Clean. Prod. 201, 272–286. https://doi.org/10.1016/J.JCLEPRO.2018.08.025.

Torres-carrasco, M., Palomo, J.G., Puertas, F., 2014. Sodium silicate solutions from

dissolution of glass wastes. Statis. Anal. Mater. Const. 64, 1–14. https://doi.org/10.3989/mc.2014.05213.
Torres-Carrasco, M., Puertas, F., 2015. Waste glass in the geopolymer preparation. Mechanical and microstructural characterisation. J. Clean. Prod. 90, 397–408. https://doi.org/10.1016/J.JCLEPRO.2014.11.074.
Van Dokkum, H.P., Hulskotte, J.H.J., Kramer, K.J.M., Wilmot, J., 2004. Emission, fate and effects of soluble silicates (waterglass) in the Aquatic environment. Environ. Sci. Technol. 38, 515–521. https://doi.org/10.1021/es0264697.
Wongsa, A., Boonserm, K., Waisurasingha, C., Sata, V., Chindaprasirt, P., 2017. Use of municipal solid waste incinerator (MSWI) bottom ash in high calcium fly ash geopolymer matrix. J. Clean. Prod. 148, 49–59. https://doi.org/10.1016/J.JCLEPRO.2017.01.147.
Xu, X., Li, Y., Yang, D., Zheng, X., Wang, Y., Pan, J., Zhang, T., Xu, J., Qiu, F., Yan, Y., Li, C., 2018. A facile strategy toward ion-imprinted hierarchical mesoporous material via dual-template method for simultaneous selective extraction of lithium and rubidium. J. Clean. Prod. 171, 264–274. https://doi.org/10.1016/J.JCLEPRO.2017.10.023.
Yan, F., Jiang, J.G., Tian, S.C., Liu, Z.W., Shi, J., Li, K.M., Chen, X.J., Xu, Y.W., 2016. A green and facile synthesis of ordered mesoporous nanosilica using coal fly ash. Acs Sustain. Chem. Eng. 4, 4654–4661. https://doi.org/10.1021/acssuschemeng.6b00793.